Supporting Information

Ultrawide-range electrochemical sensing using continuous electrospun carbon nanofibers with high densities of states

*Xianwen Mao, Xiaoqing Yang, Gregory C. Rutledge** and *T. Alan Hatton**

Department of Chemical Engineering, Massachusetts Institute of Technology
77 Massachusetts Avenue, Cambridge
Massachusetts, 02139, USA
E-mail: tahatton@mit.edu, rutledge@mit.edu

Keywords: electrochemistry, sensor, electrospinning, carbon fiber

Index for this document:

Section S1. Calculation of the sp^3/sp^2 ratios from X-ray photoelectron spectroscopy (XPS)

The high resolution XPS scans were calibrated by setting the oxygen line to 532.3 eV. The XPS C 1s sepctra were analyzed using the CasaXPS software. The background type is selected to be Shirley in order to obtain a smooth baseline, and the three components (sp^2 bonds, sp^3 bonds, and the $\pi - \pi^*$ transition peaks)[1] were fitted using a Gaussian-Lorentzian mixed shape. The fitting range is from 280 to 296 eV. The fitting results are summarized in Table S1 and Figure 2b in the main text.

Table S1. Deconvolution of the high-resolution XPS C 1s spectra.

Sample	284 eV		286 eV		288 eV	
	FWHM	**% Conc.**	**FWHM**	**% Conc.**	**FWHM**	**% Conc.**
GFs	0.58	65.3	1.67	29.6	2.65	5.1
ECNFs	0.98	44.5	2.06	31.2	6.46	24.3

Section S2. Calculation of the R_I-values from Raman spectroscopy

The Raman spectra were analyzed using the LabSpec 5 software. The baseline correction of the spectra was implemented using a polynomial with a degree of three. The D and G peaks were fitted using a Gaussian-Lorentzian mixed shape. The Raman spectrum for PAN-derived less-ordered SCHD-CNFs was deconvoluted into three bands at 1338 cm^{-1} (the D band), 1584 cm^{-1} (the G band), and 1481 cm^{-1} (the D″ band, associated with interstitial defects).[2] The Raman spectrum for the highly graphitic carbon fibers was deconvoluted into two bands at 1337 cm^{-1} (the D band) and 1585 cm^{-1} (the G band). The fitting results are summarized in Figure S1 and Table S2.

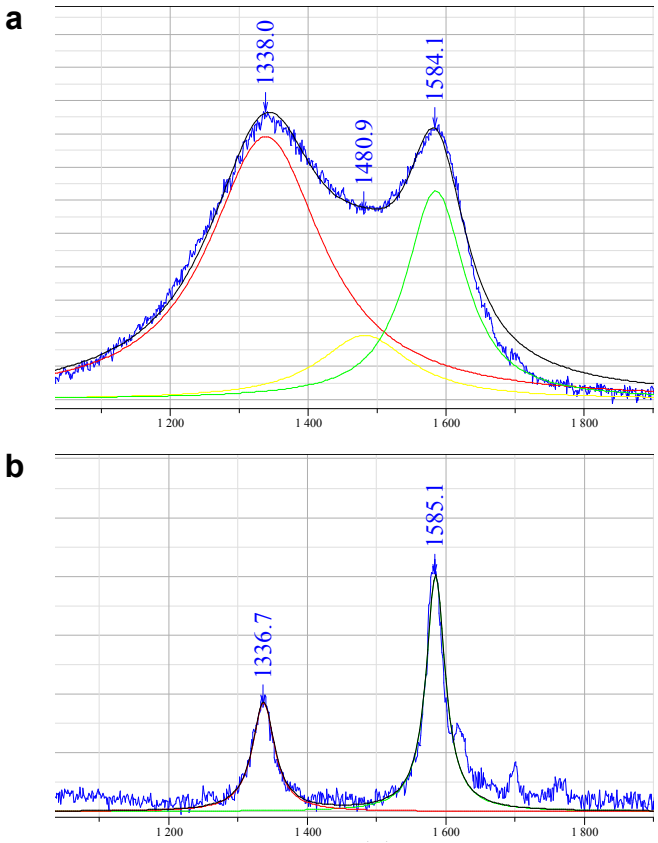

Figure S1. Raman spectra with the superposition of the fitted Gaussian-Lorentzian peaks for (a) ECNFs and (b) GFs.

Table S2. D band frequency (ν_D), D band full width at half maximum (D^{FWHM}), G band frequency (ν_G), G band full width at half maximum (G^{FWHM}), D″ band frequency ($\nu_{D''}$), D″ band full width at half maximum (D''^{FWHM}), and I_D/I_G ratio for GFs and ECNFs.

Sample	ν_D (cm^{-1})	D^{FWHM} (cm^{-1})	ν_G (cm^{-1})	G^{FWHM} (cm^{-1})	$\nu_{D''}$ (cm^{-1})	D''^{FWHM} (cm^{-1})	I_D/I_G
GFs	1336.7	38.8	1585.1	33.5	-	-	0.47
ECNFs	1338.0	201.6	1584.1	104.4	1480.9	161.8	1.26

Section S3. CV curves of $Fe(CN)_6^{3-/4-}$ at various scan rates

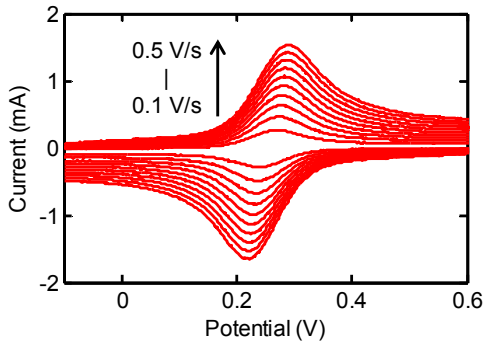

Figure S2. Cyclic voltammograms (CVs) obtained on an ECNF sensor (12 h) at scan rates from 0.1 to 0.5 V/s in the presence of 1 mM $Fe(CN)_6^{3-/4-}$.

Section S4. Decay of the current response after multiple CV scans

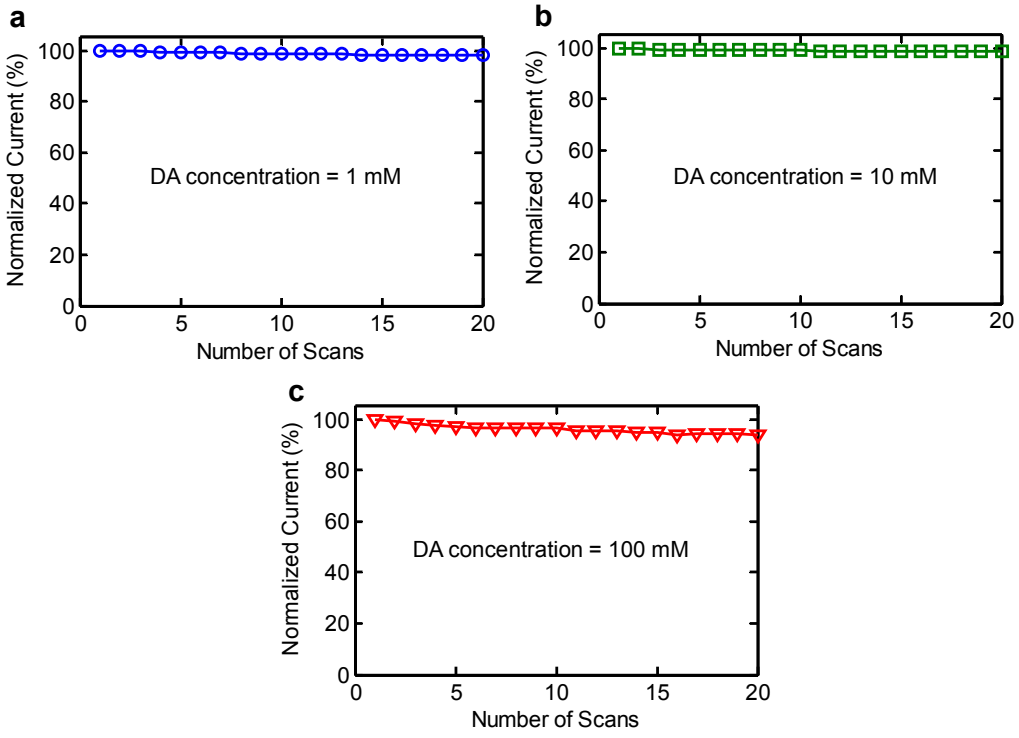

Figure S3. Decay of the anodic peak currents from the CV measurements using an ECNF sensor with 12 h deposition time in the presence of (a) 1 mM dopamine, (b) 10 mM dopamine and (c)

100 mM dopamine. The current value is normalized to the magnitude of the initial anodic peak current obtained during the first CV scan. The scan rate for all the CV measurements is 0.05 V/s.

Section S5. Selectivity of the ECNF sensors

For the selectivity of electrochemical DA sensors, a major challenge is to eliminate the interference from ascorbic acid (AA),[3-8] which coexists with DA in brain tissues and biological fluids, and exhibits an oxidation peak potential very close to that of DA at conventional electrodes such as Au, Pt, and glassy carbon electrode.[9] The highly graphitic carbon fibers (GFs) alone with very few edge sites cannot effectively distinguish between the voltammetric responses of DA and AA. The cyclic voltammograms (CVs) obtained on the bare GF substrate in the presence of 0.5 mM DA and 0.5 mM AA, respectively, are shown in Figure S4a. We observe that the GF substrate exhibits ill-defined redox waves for DA and AA, suggesting very sluggish electron transfer kinetics. Both species show overlapping oxidation voltammetric responses around 0.8-1 V on the GF substrate. This indicates that the GF substrate has very low electrochemical activity towards the two species and cannot effectively distinguish between them.

Figure S4b shows the CV curves obtained on an ECNF sensor in the presence of 0.5 mM DA and 0.5 mM AA, respectively. It can be clearly seen that the ECNF sensor exhibits a well-defined voltammetric response for 0.5 mM dopamine, showing a sharp oxidation peak at 0.55 V. Moreover, AA at the same concentration of 0.5 mM as DA shows a small oxidation peak at 0.29 V. The magnitude of the current response from AA is significantly lower than that from DA, and the oxidation peaks from the two species are well-separated. This indicates that ECNF sensor is highly effective in eliminating the interference from AA when detecting DA.

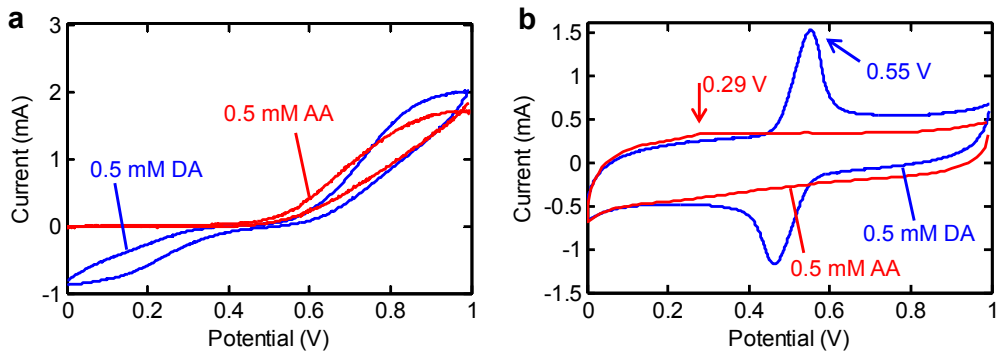

Figure S4. (a) Cyclic voltammograms obtained on the GF substrate in the presence of 0.5 mM DA (blue) and 0.5 mM AA (red), respectively. (b) Cyclic voltammograms obtained on an ECNF sensor in the presence of 0.5 mM DA (blue) and 0.5 mM AA (red), respectively.

Furthermore, we use differential pulse voltammetry (DPV), a more sensitive technique than cyclic voltammetry, to compare the current response and oxidation potentials of DA and AA obtained on the ECNF sensor. The DPV profiles in the presence of 0.5 mM DA, 0.5 mM AA, and 5 mM AA + 0.5 mM DA, respectively, are shown in Figure S5. 0.5 mM DA shows a well-shaped oxidation peak at 0.55 V whereas 0.5 mM AA displays a minor current response at 0.29 V. This observation is consistent with the CV analysis shown in Figure S4b. More importantly, a mixture containing 0.5 mM DA and 5 mM AA (at a concentration 10 times higher than that of DA) exhibits two well-resolved voltammetric peaks at 0.55 and 0.29 V, corresponding to oxidation of DA and AA, respectively. This peak separation value of 260 mV between DA and AA represents one of the best resolutions reported for the two interfering species, exceeding, for instance, a recently-reported value of 229.9 mV obtained on a graphene oxide nanoribbon electrode.[10] In addition, it can be observed in Figure S5 that the voltammetric response of 0.5 mM DA obtained on the ECNF sensor is almost the same with and without 5 mM AA. This implies that the existence of AA at a very high concentration does not interfere strongly with the detection of DA.

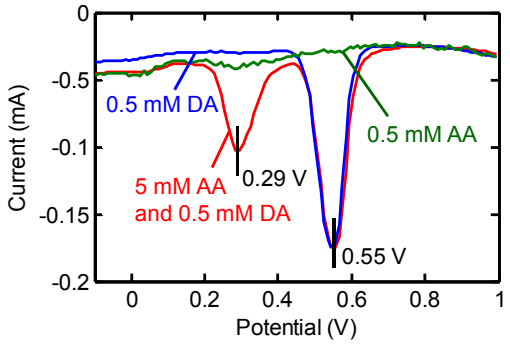

Figure S5. Differential pulse voltammograms obtained on an ECNF sensor in the presence of 0.5 mM DA (blue), 0.5 mM AA (green), and 5 mM AA + 0.5 mM DA (red), respectively.

Section S6. Discussion on the planar-diffusion behavior of $Fe(CN)_6^{3-/4-}$ of on the ECNF sensor during voltammetric measurements

We believe that, during our voltammetric measurements, the current response was controlled by planar diffusion of redox molecules present between the fibers or inside the "pores" in the fibrous mat. The inter-fiber distance is large enough (~ 1 μm, as shown in Figure 1b and 1c) to allow easy diffusion of redox molecules.

Zhang *et al.*[11] have shown that it is legitimate to use CV measurements with sufficiently high scan rates and the Randles-Sevcik equation to measure the surface area of the "nanopore" electrode. Specifically, they found that the voltammetric response (when scan rate is >= 10 mV/s) of a nanopore electrode (schematically shown in Figure S6) is limited by planar diffusion of redox molecules. They also show that CV experiments and Randles-Sevcik equation can be used to measure the electrode surface area.

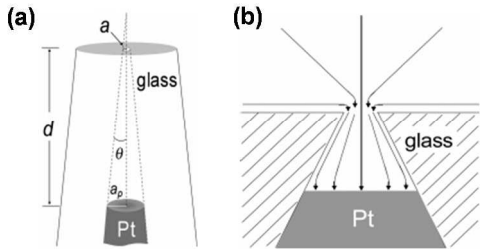

Figure S6. (a) Drawn-to-scale schematic of the nanopore electrode used by Zhang et al.[11] with a = 50 nm, d = 25 μm and θ = 20°. (b) Schematic of the flux of a redox species into the pore. Adapted from reference [11].

We think that it is reasonable to assume that in our ECNF fiber mat with large pores and inter-fiber distances, diffusion of redox species should be much easier than the case shown in Figure S6(a). In addition, in our CV measurements, we used scan rates from 100 to 500 mV/s, much higher than those used for the nanopore electrode. Therefore, the current response of our ECNF mat should be limited by planar diffusion of redox molecules inside the "pores" defined by the inter-fiber distance. Therefore, we concluded that we are indeed measuring the entire active surface area of the electrode, not just the projected area of the mesh.

This conclusion is further supported by our observation that the measured electroactive surface area (ESA) of the ECNF sensor increases significantly and scales linearly with deposition time (Figure 3e in the main text). Such an observation indicates that the ESA increases with the quantity of fibers deposited. If we were just measuring the projected area, the ESA value would be roughly the same for electrodes fabricated with different deposition times, because the nominal, geometrical area of each electrode is kept the same (0.25 cm^2); however, this is not the case in our experiments. Additionally, our measured ESA (e.g., 3.7 cm^2) is much higher than the nominal surface area of the electrode (0.25 cm^2), which also suggests that we are not just measuring the projected surface area.

The ESAs of several other types of highly porous electrodes composed of nanosized materials[12, 13] (Figure S7) have been successfully measured by CV with high scan rates and the Randles-Sevcik equation. In both reports,[12, 13] the authors showed that the CV current responses of these electrode are governed by the planar diffusion of redox species and the measured ESAs of these porous electrodes are significantly higher than the nominal surface area of the support electrode. These porous electrodes are structurally similar to our ECNF electrode, and the pores and the inter-tube distances in these electrodes are even smaller than those of the ECNF electrode. Therefore our ECNF electrode should exhibit lower transport resistances for redox species.

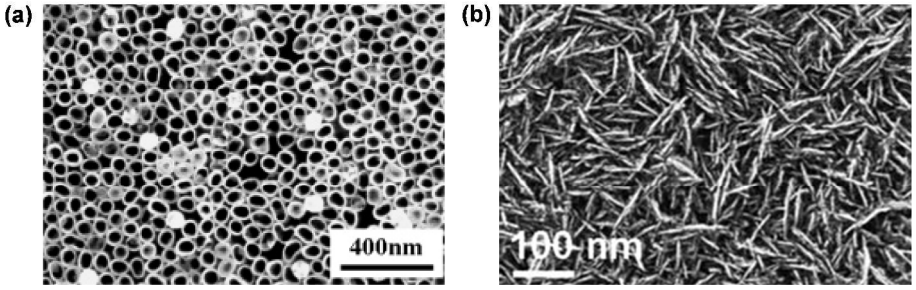

Figure S7. (a) Representative scanning electron microscopy (SEM) image of a silicon nanotube array/gold electrode.[12] Adapted from reference [12]. (b) Representative SEM image of a nitrogen incorporated diamond nanowire electrode.[13] Adapted from reference [13].

In addition, we also used chronoamperometry to determine the ESA of an ECNF sensor with 12 h deposition based upon the integrated form of the Cottrell equation:

$$Q = \frac{2nFAD^{0.5}Ct^{0.5}}{\pi^{0.5}}$$

where Q is the charge flow (mC), A is the ESA of the electrode investigated (cm^2), D is the diffusion coefficient of ferricyanide (7×10^{-6} cm^2/s),[13] n is the number of electrons transferred in the redox reaction of $Fe(CN)_6^{3-/4-}$, C is the concentration of ferricyanide in the bulk solution (M), and F is the Faraday constant. The ESA value is calculated from the slope of the Q vs. $t^{1/2}$

linear regression equation. A representative Q vs. $t^{1/2}$ plot and the linear fit are shown in Figure S8. The ESA of the ECNF sensor determined by chronoamperometry is 3.9 ± 0.5 cm^2, which agrees with the value determined by cyclic voltammetry (3.7 ± 0.4 cm^2).

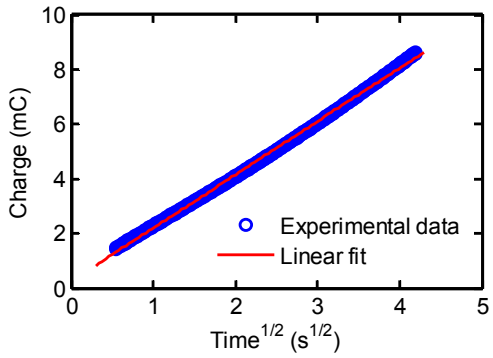

Figure S8. The total charge flow versus $t^{1/2}$ and the corresponding linear fit. The potential is increased from 0 to 0.6 V.

Section S7 Dynamic range test for the GF electrode

As a control experiment, we carried out a dynamic range test for the GF electrode. As shown in Figure S9, we recorded the CV responses of a GF electrode (nominal surface area: 0.25 cm^2) when the dopamine concentration was increased from 1 to 360 μM. The CV curves for the GF electrode are ill-shaped compared to the CV curves for the ECNF sensor. Also, there are no current responses when the dopamine concentration is below 30 μM, indicating that the GF electrode displays a very low sensitivity towards dopamine detection. In addition, we observe (Figure S9 inset) that the current magnitude becomes saturated when the dopamine concentration is around 300 μM. This observation suggests that the GF electrode exhibits a much narrower dynamic range than does the ECNF sensor. The low activities of the GF electrode is attributed to its low edge site density, low DOS, and small surface area reflected by its low capacitance.

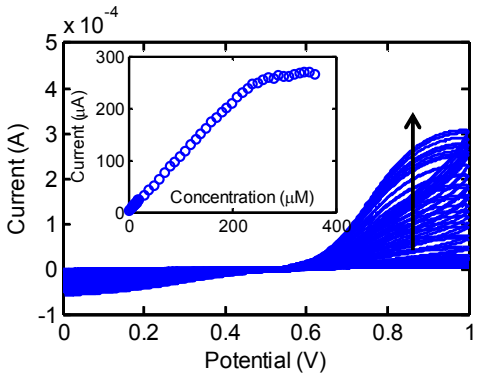

Figure S9. Cyclic voltammetric responses of a GF electrode (nominal surface area: 0.25 cm^2) in the presence different dopamine concentrations. With the arrow direction, the dopamine concentration increases from 1 to 360 μM. Scan rate: 50 mV/s. Inset: the magnitude of the anodic current at 0.9 V as a function of dopamine concentration.

Section S8 Measurement of the capacitances of the GF electrode and the ECNF sensor

We measured the capacitances of an ECNF sensor with 12 h deposition and a GF electrode using cyclic voltammetry in 1 M H_2SO_4 (see Figure S10) based on the following equation:[14]

$$C = \int_{V_1}^{V_2} [i_a(V) - i_c(V)]dV \Big/ [2(V_2 - V_1)v] \qquad (1)$$

where is the gravimetric capacitance of the sample, V_1 and V_2 are the cutoff potentials in cyclic voltammetry, $i_a(V)$ and $i_c(V)$ are the instantaneous anodic and cathodic currents as a function of potential, and v is the scan rate, and A is the total surface of the active materials on one electrode. Equation (1) is a universal expression that applies to cyclic voltammograms of any shape since it uses the integral area of the cyclic voltammogram/scan rate to represent the sum of anodic and cathodic voltammetric charges.[14]

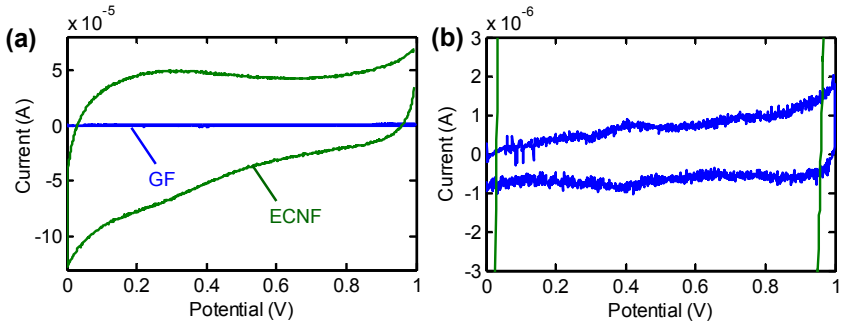

Figure S10. (a) Cyclic voltammograms of the GF electrode and an ECNF sensor with 12 h deposition at a scan rate of 50 mV/s in 1 M H_2SO_4. (b) Enlarged view of panel (a) to show the cyclic voltammogram of the GF electrode.

We normalized the calculated capacitances of the GF electrode and the ECNF sensor with respect to the nominal surface area of the electrode (0.25 cm^2); the normalized capacitance for the GF electrode and the ECNF sensor is 54 and 3600 $\mu F/cm^2$, respectively. It is clear that the ECNF sensor exhibits a much higher surface area than does the GF electrode. Note that dopamine is an "inner-sphere" species whose redox reaction is surface-sensitive and adsorption-assisted; thus, a large electrode surface area increases electron transfer efficiencies with DA and results in enhanced sensitivity.[15] The GF electrode exhibits a very low activity towards DA. In addition, for the ECNF sensors fabricated with different depositions times, the detection limit improves when the deposition time increases from 5 to 12 h.

References for the Supporting Information

[1] H. Estrade-Szwarckopf, *Carbon* **2004**, *42*, 1713.
[2] C. Kim, S. H. Park, J. K. Cho, D. Y. Lee, T. J. Park, W. J. Lee, K. S. Yang, *J Raman Spectrosc* **2004**, *35*, 928.
[3] Y. R. Kim, S. Bong, Y. J. Kang, Y. Yang, R. K. Mahajan, J. S. Kim, H. Kim, *Biosens Bioelectron* **2010**, *25*, 2366.
[4] Y. Wang, Y. M. Li, L. H. Tang, J. Lu, J. H. Li, *Electrochem Commun* **2009**, *11*, 889.
[5] X. H. Cao, L. X. Zhang, W. P. Cai, Y. Q. Li, *Electrochem Commun* **2010**, *12*, 540.
[6] S. F. Hou, M. L. Kasner, S. J. Su, K. Patel, R. Cuellari, *J Phys Chem C* **2010**, *114*, 14915.
[7] X. W. Kan, Y. Zhao, Z. R. Geng, Z. L. Wang, J. J. Zhu, *J Phys Chem C* **2008**, *112*, 4849.
[8] S. Shahrokhian, H. R. Zare-Mehrjardi, *Electrochim Acta* **2007**, *52*, 6310.
[9] C. Y. Deng, J. H. Chen, M. D. Wang, C. H. Xiao, Z. Nie, S. Z. Yao, *Biosens Bioelectron* **2009**, *24*, 2091.
[10] C. L. Sun, C. T. Chang, H. H. Lee, J. G. Zhou, J. Wang, T. K. Sham, W. F. Pong, *Acs Nano* **2011**, *5*, 7788.
[11] B. Zhang, Y. H. Zhang, H. S. White, *Anal Chem* **2006**, *78*, 477.
[12] C. Mu, Q. Zhao, D. S. Xu, Q. K. Zhuang, Y. H. Shao, *J Phys Chem B* **2007**, *111*, 1491.
[13] J. Shalini, K. J. Sankaran, C. L. Dong, C. Y. Lee, N. H. Tai, I. N. Lin, *Nanoscale* **2013**, *5*, 1159.
[14] W. Chen, Z. L. Fan, L. Gu, X. H. Bao, C. L. Wang, *Chem Commun* **2010**, *46*, 3905.
[15] R. L. McCreery, *Chem Rev* **2008**, *108*, 2646.